



## RESEARCH ARTICLE

10.1029/2023JD040434

# Multiscale CO Budget Estimates Across South America: Quantifying Local Sources and Long Range Transport

### Key Points:

- We employ the Multi-Scale infrastructure for Chemistry and Aerosols to quantify the budget of CO in South America during 2019
- Most of the variability in the CO burden is explained by the variability in biomass burning emissions
- Biomass burning in Central Africa is a relevant contributor to CO in all of the continent, including the southern region

### Supporting Information:

Supporting Information may be found in the online version of this article.

### Correspondence to:

G. P. Brasseur and P. Lichtig,  
guy.brasseur@mpimet.mpg.de;  
pablolichtig@cnea.gov.ar

### Citation:

Lichtig, P., Gaubert, B., Emmons, L. K., Jo, D. S., Callaghan, P., Ibarra-Espinosa, S., et al. (2024). Multiscale CO budget estimates across South America: Quantifying local sources and long range transport. *Journal of Geophysical Research: Atmospheres*, 129, e2023JD040434. <https://doi.org/10.1029/2023JD040434>

Received 14 NOV 2023

Accepted 24 MAR 2024

### Author Contributions:








**Conceptualization:** Pablo Lichtig, Benjamin Gaubert, Guy P. Brasseur, Gabriele Pfister

**Data curation:** Pablo Lichtig, Gabriele Pfister

**Formal analysis:** Pablo Lichtig, Benjamin Gaubert, Louisa K. Emmons, Duseong S. Jo, Guy P. Brasseur, Gabriele Pfister

**Funding acquisition:** Guy P. Brasseur, Gabriele Pfister

**Investigation:** Pablo Lichtig, Benjamin Gaubert

Pablo Lichtig<sup>1,2</sup> , Benjamin Gaubert<sup>3</sup> , Louisa K. Emmons<sup>3</sup> , Duseong S. Jo<sup>3</sup> , Patrick Callaghan<sup>3</sup>, Sergio Ibarra-Espinosa<sup>4</sup> , Laura Dawidowski<sup>1</sup>, Guy P. Brasseur<sup>5</sup> , and Gabriele Pfister<sup>3</sup> 

<sup>1</sup>National Commission of Atomic Energy, Buenos Aires, Argentina, <sup>2</sup>National Counsel of Science and Technology, Buenos Aires, Argentina, <sup>3</sup>NSF National Center for Atmospheric Research, Boulder, CO, USA, <sup>4</sup>National Oceanographic and Atmospheric Administration, Boulder, CO, USA, <sup>5</sup>Max Planck Institute for Meteorology, Hamburg, Germany

**Abstract** South America is a large continent situated mostly in the Southern Hemisphere (SH) with complex topography and diverse emissions sources. However, the atmospheric chemistry of this region has been historically understudied. Here, we employ the Multi-Scale Infrastructure for Chemistry and Aerosols, a novel global circulation model with regional refinement capabilities and full chemistry, to explore the sources and distribution of the carbon monoxide (CO) tropospheric column in South America during 2019, and also to assess the effect that South American primary emissions have over the rest of the world. Most of the CO over South America can be explained either by non-methane volatile organic compounds (NMVOC) secondary chemical production or by biomass burning emissions, with biomass burning as the main explanation for the variability in CO. Biomass burning in Central Africa is a relevant contributor to CO in all of the continent, including the southern tip. Biogenic emissions play a dual role in CO concentrations: they provide volatile organic compounds that contribute to the secondary CO production, but they also destroy OH, which limits the chemical production and destruction of CO. As a net effect, the lifetime of CO is extended to ~120 days on average over the Amazon, while still being in the range of 30–60 days in the rest of South America.

**Plain Language Summary** We use the Multi-Scale Infrastructure for Chemistry and Aerosols, a global model with regional refinement, to study the origins of carbon monoxide (CO) in South America during 2019. The main sources of CO are the secondary production from non-volatile organic compounds and the biomass burning primary emissions. The main source of temporal variability in the whole are the biomass burning emissions. We show that biomass burning in central Africa is a relevant source of South American CO during all year in all of the continent, including the furthestmost south.

## 1. Introduction

Carbon monoxide (CO) is an atmospheric trace gas constituent that plays an important role in tropospheric chemistry (Gaubert et al., 2017; Levy, 1971). Globally, the CO primary sources result from incomplete combustion of fossil fuel from industrial, road transportation and residential sectors, and from biomass burning, including for cooking, heating and wildfires (Duncan et al., 2007). Other minor sources include biological processes, mainly by land's vegetation, with minor contributions from oceanic emissions. The CO oxidation into CO<sub>2</sub> (Equation 1) plays an essential role in atmospheric chemistry as a major sink of hydroxyl radical (OH), and a source of hydroperoxyl radical (HO<sub>2</sub>) (Stone et al., 2012). CO has a relatively long lifetime (weeks to months), and is mostly emitted by anthropogenic emissions or biomass burning (Gaubert et al., 2016). Hence, it is often used as a tracer for pollution sources and transport, and will be the main focus of this study (Edwards, 2004).



Around 50% of CO is formed in the atmosphere as a result of the oxidation of methane (CH<sub>4</sub>) and non-methane volatile organic compounds (NMVOCs) (Duncan et al., 2007; Gaubert et al., 2016; Stein et al., 2014), either through photolysis or through multiple oxidation process. Aside from photolysis, most organic compounds including CH<sub>4</sub> and NMVOCs are oxidized mainly or exclusively by OH (Seinfeld & Pandis, 2016), as shown in Equation 2. The oxidation process by OH produces organic peroxy radicals (RO<sub>2</sub>), which can later produce CO through multiple reaction pathways.

© 2024. The Authors.

This is an open access article under the terms of the [Creative Commons Attribution License](https://creativecommons.org/licenses/by/4.0/), which permits use, distribution and reproduction in any medium, provided the original work is properly cited.

**Methodology:** Pablo Lichtig,  
Benjamin Gaubert, Patrick Callaghan, Guy  
P. Brasseur, Gabriele Pfister

**Project administration:** Guy P. Brasseur,  
Gabriele Pfister

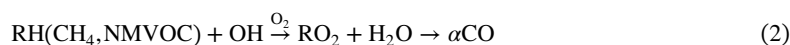
**Resources:** Laura Dawidowski, Guy  
P. Brasseur, Gabriele Pfister

**Supervision:** Guy P. Brasseur,  
Gabriele Pfister

**Validation:** Pablo Lichtig,  
Benjamin Gaubert, Louisa K. Emmons,  
Duseong S. Jo, Gabriele Pfister

**Visualization:** Pablo Lichtig  
**Writing – original draft:** Pablo Lichtig,  
Benjamin Gaubert

**Writing – review & editing:**  
Pablo Lichtig, Benjamin Gaubert, Louisa  
K. Emmons, Duseong S. Jo, Sergio Ibarra-  
Espinosa, Laura Dawidowski, Guy  
P. Brasseur, Gabriele Pfister



The yield  $\alpha$  varies according to oxidation pathways, including the  $\text{NO}_x$  levels, and products generated (Grant et al., 2010; Pfister et al., 2008). Therefore, the net effect of a change in OH on the CO budget is not always straightforward, as OH acts both as a source and a sink for CO (Gaubert et al., 2016, 2017).

CO has been studied extensively in the Northern Hemisphere where even the background levels are almost twice as large as in the Southern Hemisphere (Novelli, 2003). Comparisons with the satellite CO observations indicate that global models have remaining difficulties to simulate CO during the winter and spring with a strong underestimation in the Northern Hemisphere extratropics (Shindell et al., 2006), mostly because of underestimation in emissions (Gaubert et al., 2020; Stein et al., 2014) and representation of the chemistry (Gaubert et al., 2023; Müller et al., 2018; Naik et al., 2013). High CO amounts from biomass burning were first observed in the 1990's from the Measurement of Air Pollution from Satellites (MAPS) experiment (Watson et al., 1990). Biomass burning emissions are the main driver of CO levels in the tropics and in the Southern Hemisphere, explaining the inter-model differences in modeled CO levels, with a strong interannual variability (Edwards, 2004; Shindell et al., 2006).

As reported by Paton-Walsh et al. (2022), the Southern Hemisphere, in contrast, remains largely understudied. It holds only  $\sim 10\%$  of the global population, and is  $\sim 80\%$  ocean. There, biomass burning and biogenic emissions are of high importance. It also holds the cleanest atmospheric conditions, found in the Southern Ocean. Park et al. (2013) have characterized that secondary CO derived from NMVOCs can be highly variable. They found that in the Southern Hemisphere, the secondary CO produced by NMVOC is not highly correlated with temperature, but with El Niño Southern Oscillation (ENSO).

South America is a continent extending from  $55.8^\circ\text{S}$  to  $12.5^\circ\text{N}$  and  $81.4^\circ\text{W}$ – $34.3^\circ\text{W}$ . It has a large variety of vegetation, soil and climate regions (de Miranda et al., 2022), ranging from the rainforests in the Amazon Basin to the desert in Atacama, the plains in the Pampas, the Patagonian Steppe and the continental ice of southern Chile. Most of the previous studies in South America have been conducted over the Amazon rainforest and basin. Zheng et al. (2021) reported an increase in fire emissions since 2013, based on satellite observations. Naus et al. (2022) have done an extensive study of fire emissions in the Amazon from 2003 to 2018, as part of their inverse modeling efforts. They found strong seasonal patterns in CO emissions, as well as probable negative biases in fire emission inventories. In their global study, Buchholz et al. (2021) found no significant trend for the dry-air column-averaged mole fraction of CO in the Amazon during the period 2002–2018. They also took into account a region over the ocean close to the continent, in which they detected a positive trend, mostly during the first half of that period (2002–2010). In terms of the seasonal cycle, they found peak CO column concentrations during the fire season (August–November), with a clear maximum in September of about 140 ppbv, averaged over the Amazon. Over the Ocean close to South America, that maximum is spread over October and September. To avoid the problem of averaging over regions, Hedelius et al. (2021) estimated the dry-air column-averaged mole fraction and trends globally, in a  $0.4^\circ \times 0.4^\circ$  grid. The mean dry-air column-averaged mole fraction of CO during 2002–2017 in South America spanned from  $\sim 110$  ppbv in the Amazon to  $\sim 50$  ppbv in the southern tip. The trend found by them was mostly negative ( $\sim -0.5\%$ ), except for the region west of the Andes and south of the Equator, in which it was very slightly positive. However, when separated into 5 year periods, they found a positive trend in 2013–2017 over the whole continent, spanning 0%–4%. They also report that the EDGAR emission inventory shows an increase in anthropogenic emissions during the period 2002–2012 in all of the continent. All these studies show that the natural sources in the Southern Hemisphere are highly variable.

The goal of this study is to quantify the local and long range origins of CO in South America using model diagnostics and CO tagged tracers. We utilize the newly developed Multi-Scale Infrastructure for Chemistry and Aerosols version 0 (MUSICAv0) (Pfister et al., 2020; Schwantes et al., 2022) with regional mesh refinement over South America. This study is the first that applies MUSICAv0 over South America. We employ a system of CO tagged tracers to quantify the CO budget for the year 2019 and to identify geographical origins of CO by sources.

In Section 2, we first describe the general model setup (subsec. 2.1) and a CO tagged tracer mechanism (subsec. 2.2). We then describe the evaluation of the model results using satellite data (subsec. 2.3) and the methodology to evaluate CO sources and CO variability using the tags (subsec. 2.4). In Section 3, we start by evaluating the model with satellite CO data (subsec. 3.1). We then evaluate the CO budget both globally and over

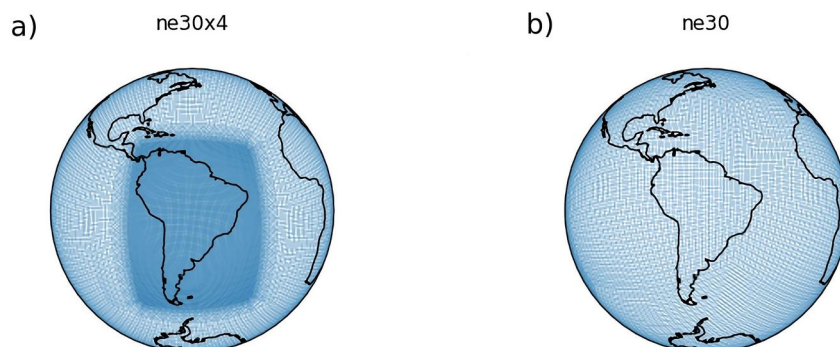


**Figure 1.** Model meshes.

South America, and compare the results of the MUSICAv0 refined simulation with a standard, control run with a global coarse grid (subsec. 3.2). In Section 3.3, we analyze the effect on the burden and the variability, as well as the spatial distribution of the CO chemical lifetime. We further discuss the variability and geographical origin of CO in 3.3.2. In Section 3.3.3, we analyze the effect that South American primary emissions are having in the CO burden over the rest of the world. Finally, we summarize our results and conclusions in Section 4, and close the paper discussing future perspectives. Links to all the original data are provided in the Open Research section.

## 2. Methods

### 2.1. Model Description and Setup

We use MUSICAv0, which is part of the Community Earth System Model (Danabasoglu et al., 2020) version 2.2 (CESM2.2), an open source Earth System Model maintained by the National Center for Atmospheric Research (NCAR). MUSICAv0 is a configuration of the Community Atmosphere Model with Chemistry (CAM-chem) (Emmons et al., 2020; Tilmes et al., 2019) with a spectral element (SE) dynamical core that allows for regional refinement (Lauritzen et al., 2018; Schwantes et al., 2022; Tang et al., 2022, 2023). The model is run coupled to the Community Land Model (CLM) v5.0 (Lawrence et al., 2019) to interactively simulate land processes, the deposition of gases and aerosols and biogenic emissions. The latter are estimated from the Model of Emissions of Gases and Aerosols from Nature (MEGAN) version 2.1 (Guenther et al., 2012) and depend interactively on the modeled temperature, solar radiation, leaf area index (LAI) and other modeled parameters. We employ prescribed monthly LAI at 0.25° resolution, denoted as satellite phenology. The effect resulting from this configuration is discussed in detail in Jo et al. (2023). We note that the MEGAN emissions are calculated in whichever form they leave the canopy. Sometimes, quick reactions can occur before this happens, leading to the presence of “primary” biogenic emissions of species that are not, in fact, directly emitted by the plants (of particular importance for this work, CO is one of these species). In this paper, we perform a global simulation including a mesh refinement over South America ( $ne30 \times 4$  [ $\sim 28$  km]) and a control simulation at uniform resolution ( $ne30$  [ $\sim 111$  km]), as shown in Figure 1. Unless otherwise stated for specific parameters, the two simulations should be assumed to have the same setup. The  $ne30$  simulation is run with a physical time step of 1800 s, while the  $ne30 \times 4$  simulation uses a time step of 450 s. Both simulations have 32 vertical layers, with  $\sim 7$  model layers below the planetary boundary layer height (PBLH) and  $\sim 15$  layers below the stratosphere, and a hybrid terrain following vertical coordinate. The Cloud Layers Unified by Binormals (CLUBB) scheme is used for shallow convection, cloud microphysics and boundary layer turbulence (Bogenschutz et al., 2013), and the MG2 scheme is used for cloud microphysics (Gettelman & Morrison, 2015). The ZM scheme (Zhang & McFarlane, 1995) is used for deep convection. We nudge relevant meteorological parameters (T, U, V) to the Modern-Era Retrospective Analysis for Research and Applications, Version 2 (MERRA-2) (Gelaro et al., 2017), with a 12 hr relaxation time.

As a chemical mechanism, we employ the Model for Ozone and Related Chemical Tracers with tropospheric and stratospheric chemistry (MOZART-TS1) (Emmons et al., 2020) and the Modal Aerosol Model with 4 modes (MAM4) (Liu et al., 2016). We use anthropogenic emissions from the CAMS-GLOB-ANT version 5.3, and aircraft emissions from CAMS-GLOB-AIR version 2.1 (Soulie et al., 2023). The daily fire emissions are prescribed from the Fire Inventory from NCAR version 2.5 (FINN2.5), using both MODIS and VIIRS fire detection (Wiedinmyer et al., 2023). The chemistry mechanism also includes a volatility basis set representation of

**Table 1**  
Global and Latitudinal CO Tags

CO tag	Geogr. origin	Source
CO <sub>ant</sub>	World	Anthropogenic emissions
CO <sub>bb</sub>	World	Biomass burning emissions
CO <sub>ocn</sub>	World	Ocean emissions
CO <sub>bio</sub>	World	Biogenic emissions from land
CO <sub>met0.75</sub>	World	Sec. Methane (yield = 0.75)
CO <sub>met1</sub>	World	Sec. Methane (yield = 1)
CO <sub>bbSET</sub>	lat: 90°S–24°S	Biomass burning emissions
CO <sub>bbST</sub>	lat: 24°S–0°	Biomass burning emissions
CO <sub>bbNT</sub>	lat: 0°N–24°N	Biomass burning emissions
CO <sub>bbNET</sub>	lat: 24°N–90°N	Biomass burning emissions
CO <sub>antSET</sub>	lat: 90°S–24°S	Anthropogenic emissions
CO <sub>antST</sub>	lat: 24°S–0°S	Anthropogenic emissions
CO <sub>antNT</sub>	lat: 0°–24°N	Anthropogenic emissions
CO <sub>antNET</sub>	lat: 24°N–90°N	Anthropogenic emissions

secondary organic aerosol (Tilmes et al., 2019) with nitrogen oxides (the sum of nitrogen monoxide and nitrogen dioxide, NO<sub>x</sub>) dependent pathways for secondary organic aerosol (SOA) formation (Jo et al., 2021). We include the update of the HO<sub>2</sub> heterogeneous uptake introduced by Gaubert et al. (2020).

The spin-up simulations for the land model and the atmospheric model are performed separately. The land model is spun-up for a year at the final resolution, with a default CESM/CAM simulation initialized from long-term CESM2.2 simulation. The atmospheric chemistry spin-up is run in a ne30 configuration, also for a year, but with full chemistry and including the aforementioned tags. For 2019, the ne30 simulation is simply continued for the complete period. For the ne30 × 4 simulation, the model initial conditions resulting from the ne30 simulation spin-up is regridded to the finer grid, and run together for a month with the output of the land spin-up, as a final spin-up step. The simulation is then continued for the entire year of 2019.

## 2.2. CO Tagged Tracers

We include a series of CO tagged tracers (hereafter CO tags) to identify transport of different sources. This approach has been previously used with various chemistry models (Gaubert et al., 2016; Tang et al., 2019; R. A. Fisher & Koven, 2020) to identify pollution origins and transport. The primary

tagged tracers used in this study include 4 global CO tags according to the source type (anthropogenic, biomass burning, oceanic, biogenic). The sum of the four tags define the primary CO (Equation 3).

$$\text{CO}_{\text{primary}} = \text{CO}_{\text{ant}} + \text{CO}_{\text{bb}} + \text{CO}_{\text{ocn}} + \text{CO}_{\text{bio}} \quad (3)$$

We define the secondary CO by subtracting the primary CO from the modeled total CO (Equation 4).

$$\text{CO}_{\text{secondary}} = \text{CO} - \text{CO}_{\text{primary}} \quad (4)$$

We also define two tags to quantify the secondary CO resulting from the methane (CH<sub>4</sub>) oxidation. CH<sub>4</sub> can be a major source of secondary CO, following complex reaction paths (Gaubert et al., 2016). Duncan et al. (2007) has reported a yield approaching unity using the model GEOS-Chem version 5.02, and a yield of 1 has been used in subsequent GEOS-Chem studies (J. A. Fisher et al., 2017). Gaubert et al. (2016) found a yield of 0.75 using CAM-Chem, due to the wet deposition of intermediate soluble species. To quantify the CH<sub>4</sub> source of secondary CO, two tags were added to Equation 2 as shown in Equation 5, one with a yield of 1 and another one assuming a yield of 0.75, without altering the other products of the oxidation of CH<sub>4</sub> by OH. Since the model configuration in Gaubert et al. (2016) is closely related to the model configuration here, only the results for a yield of 0.75 are shown.



where CO<sub>met1</sub> refers to the tag with a yield of 1 and CO<sub>met0.75</sub> refers to the tag with a yield of 0.75.

Having an estimation of CO generated by methane allows us to estimate secondary CO generated by other volatile organic compounds, where isoprene is the main source of CO, as shown in Equation 6.

$$\text{CO}_{\text{nmvoc}} = \text{CO} - \text{CO}_{\text{primary}} - \text{CO}_{\text{met}} \quad (6)$$

We also define latitudinal tags for anthropogenic and biomass burning emissions, as described in Table 1. Other geographical CO tags were defined as shown in Figure 2. As in Gaubert et al. (2016), these tags are co-emitted and share the same dry deposition and chemical destruction rate as CO, but do not alter OH. We then estimate the contribution of each global source of CO (anthropogenic emissions, biomass burning emissions, emissions from the ocean, primary biogenic emissions and secondary CO). There is no specific tagged tracer for the secondary CO derived from NMVOCs, but it can be estimated as shown in Equation 6 by choosing a yield for CH<sub>4</sub>.

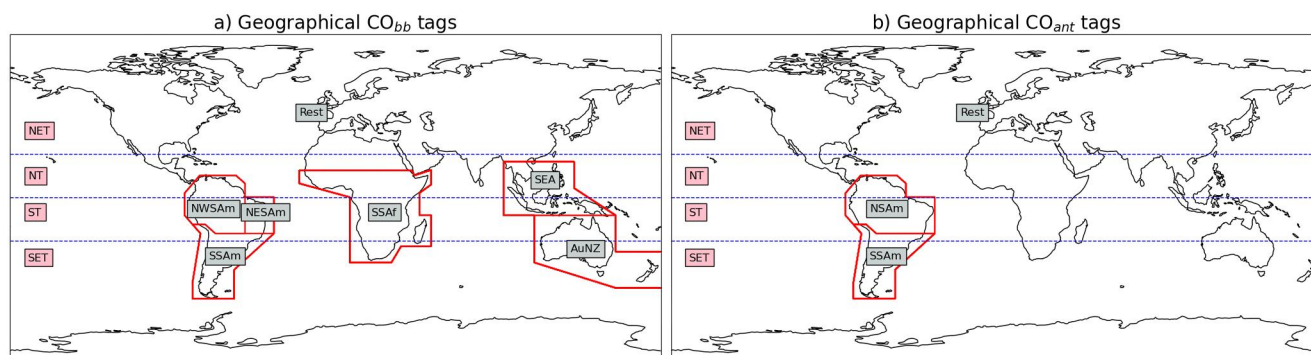


**Figure 2.** Geographical CO tags for biomass burning (bb) and anthropogenic (ant) CO (red). The latitudinal bands used for the latitudinal CO tags are also shown with a dashed blue line.

### 2.3. Model Evaluation

The model is evaluated through comparison with gridded data from the Measurement Of Pollution In The Troposphere instrument (MOPITT) Level 3 data, on board of the Terra spacecraft. These retrievals have been used extensively to evaluate model output (Daskalakis et al., 2022; Dekker et al., 2017; Gaubert et al., 2016, 2020). The output of the simulation is regridded to a  $1^\circ \times 1^\circ$  structured grid, and the MOPITT averaging kernel and a priori CO concentration are utilized as in Gaubert et al. (2016) to smooth dry-air column-averaged mole fraction (XCO) of the model in a way that can be compared to the satellite product. A simple subtraction in MOPITT space is applied for every simulated monthly mean. A similar procedure is then applied to the vertical distribution of CO, which we use to analyze a vertical cross section over the Amazon. The regionally refined model output is compared to the control (ne30) by regridding both outputs conservatively to a  $0.25^\circ$ – $0.25^\circ$  grid worldwide.

### 2.4. Evaluation of the Main Sources of CO and CO Variability

The mean tropospheric burden for each global CO tag is calculated for the complete simulation period. The standard deviation is also calculated utilizing the monthly means, to characterize the variability. The monthly means of the regional CO tags of Figure 2 are used to evaluate the regional sources of CO as the year progresses.

The chemical lifetime of CO for each month is calculated as shown in Equation 7.

$$\text{lifetime} = \text{CO}_{\text{burden}} / \text{CO}_{\text{CHML}}, \quad (7)$$

where  $\text{CO}_{\text{CHML}}$  is the integral of the CO chemical loss. Since OH is the only source of chemical loss of CO, and isoprene over the Amazon is a major source of OH loss, dry-air column averaged mole fractions of OH and isoprene are also used in the analysis to evaluate matching patterns. We expect regions with long chemical lifetimes to have low OH concentrations, which could, in some cases, be explained by high concentrations of isoprene.

Although most of South America (SAm) is in the Southern Hemisphere (SH), its northern tip stretches into the Northern Hemisphere (NH), including a portion of the Amazon rainforest. The latitudinal CO tags are used to evaluate cross-hemispheric transport, the effects that SAm might be having over each hemisphere and the effects of the NH over SAm.

The global relevance of SAm's primary emissions can be analyzed by adding the  $\text{CO}_{\text{ant}}$  and  $\text{CO}_{\text{bb}}$  tags from all the South American regions, and calculating the fraction of tagged CO over the total CO for any area of interest.

## 3. Results

### 3.1. Evaluation With MOPITT

In Figure 3, we show the ne30  $\times$  4 model bias compared to MOPITT XCO for four individual months during the year. The XCO comparison for all months can be found in the SI (Figure S1 in Supporting Information S1). The analysis for the control run yielded similar results and is shown in Figure S2 in Supporting Information S1.

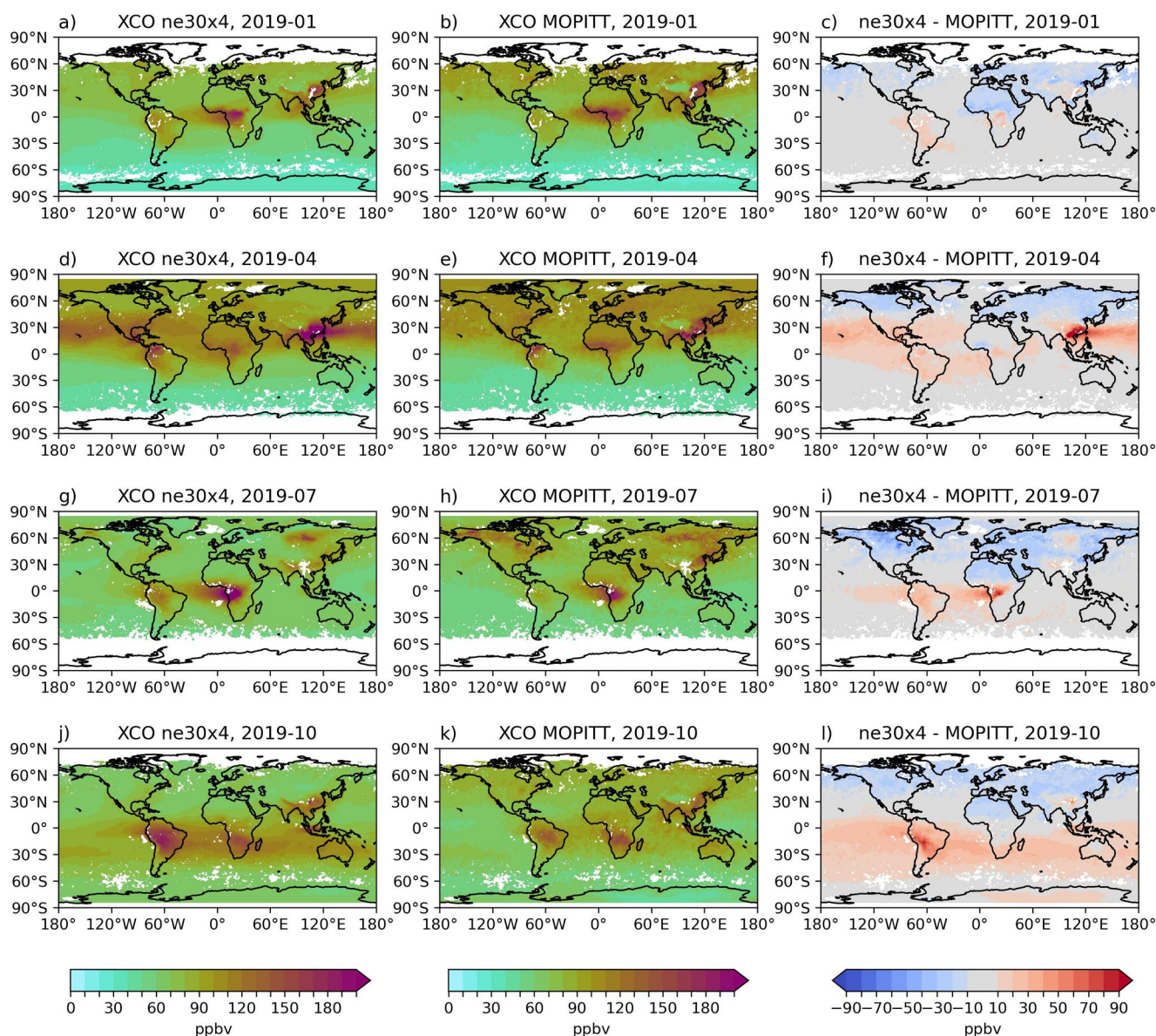


**Figure 3.** Model evaluation with MOPITT for the months of Jan, Apr, Jul, and Oct. See Figure S1 in Supporting Information S1 for the total monthly difference for every simulated month. XCO represents the dry-air column averaged mole fraction. The model XCO is calculated by regriding to MOPITT space and using the MOPITT averaging kernel.

The general distribution of global CO is well represented in terms of the location of the hotspots. However, there are distinct biases in both hemispheres.

The simulated CO in the SH is generally higher than MOPITT retrievals. This applies to all of SAM, including the part of SAM that lies in the NH region. This is especially true during the biomass burning season, which starts in August and continues until the end of the year. In most months, the bias is below 20 ppbv, however, during the fire season, it can locally reach up to 90 ppbv. This high bias decreases rapidly further away from the fire hotspot, but it can remain at about 20–30 ppbv in the whole SH. During the first months of the year, part of the CO is likely carried over from the previous months, during which strong biomass burning events and an active ENSO occurred.

The version of FINN2.5 utilized provides the highest CO and NMVOC emissions of the commonly used fire emission inventories (Wiedinmyer et al., 2023). MOPITT and MODIS assimilation have shown important and

large-scale positive biases in CO and aerosols (Gaubert et al., 2023). Some of the bias could be explained by the relative importance of the fire emissions in the SH combined with larger uncertainties in the anthropogenic emissions and the concentrations of other species (Paton-Walsh et al., 2022), including OH and biogenic NMVOC. It is unlikely that the fire inventory of choice is the only explanation, considering that Daskalakis et al. (2022), although studying a different time period, found similar bias patterns compared to MOPITT utilizing emissions from the Atmospheric Chemistry and Climate Intercomparison Project (ACCMIP) emission database and the offline chemical transport model TM4-ECPL. Positive biases in daytime compared to MOPITT data at 500 hPa were also found in CAM-Chem over the Amazon by Lamarque et al. (2012), using the emissions from the Global Fire Emissions Database (GFED) and FINN version 1 (van der Werf et al., 2010; Wiedinmyer et al., 2011).

In order to evaluate the vertical distribution, we show in Figure 4 the distribution of the bias in a vertical cross section at 60°S (which crosses the Amazon rainforest) during the same four individual months. It shows that MOPITT observations indicate upper tropospheric CO just south of the equator around 10°S, and large CO enhancement from 0° to 40°S during the fire season, mostly below ~500 hPa. The model is overestimating those higher CO values, leading to a higher bias between 700 and 300 hPa around 20°S. Uncertainties in fire emissions are one likely reason for these biases and possible biases in FINN2.5 over South America should be taken into account in future studies, considering that 2019 was relatively average in terms of fire emissions in the continent (Figure S3 in Supporting Information S1).

For additional interpretation and evaluation, we show in Figure S7 in Supporting Information S1 simulated surface CO for each month highlighting peak concentrations during the fire season. We further present a comparison to NOAA's Carbon Cycle Greenhouse Gas data set (Figure S8 in Supporting Information S1) (Petron et al., 2019), which reflects a similar spatial pattern as found in the comparison with MOPITT. Finally, we also include a vertical cross section of CO compared to MOPITT over the Atlantic (Figure S9 in Supporting Information S1), which can help analyze how CO is transported to and from Africa. There, the highest biases are at middle and higher altitudes (over 600 hPa).

### 3.2. CO Budget

Here we compare the two different simulations (ne30 and ne30 × 4) in order to assess the impacts of a refined region over SAm. The higher resolution over the refined region is expected to better represent the sources and transport, thus also leading to changes in the chemistry and CO lifetimes. Table 2 shows the CO budget at the global scale and for South America.

SAm represents about 17% of the global CO emissions and 39% of the SH CO emissions. It includes 22% of the global biomass burning emissions, but only 9% of the global anthropogenic emissions. As shown in Table 2, the overall differences between the refined and the control grids in terms of the CO burden and budget estimates are fairly small.

There are, however, differences in the spatial distribution of the CO burden (Figure 5). A small part of the differences far from the refined region can be due to global changes in the process of creating the ne30 × 4 grid, which has minor differences with ne30 even far away from the refined region (i.e., a rotation of the cubed sphere used by the Spectral Elements dynamical core). Most of the differences, however, are likely due to changes in the refined region, that could have global impacts either directly or indirectly due to meteorological feedbacks and transport. The mean dry-air column averaged OH mole fraction over the South-American continent is about the same in both simulations (0.64 ppt in ne30 vs. 0.63 in ne30 × 4) but shows differences spatially (Figure S4 in Supporting Information S1). When analyzing the different components of the budget, it is clear that the differences are mostly due to differences in chemical production and loss. The ne30 × 4 simulation has generally larger OH concentrations over the Andes, but smaller OH concentrations elsewhere. The CO burden in the ne30 × 4 simulation is smaller than the ne30 simulation to the west of the Andes, but larger to the east. Analyzing every CO tag, we find that the CO<sub>nmvoc</sub> burden is actually smaller in the ne30 × 4 simulation on both sides of the Andes, likely due to less CO being produced from the oxidation of NMVOCs by OH. However, the CO<sub>bb</sub> burden in the ne30 × 4 simulation is generally larger in the ne30 simulation over the continent. This is likely also the effect of less OH over the Amazon, and therefore less oxidation of CO<sub>bb</sub>. When CO<sub>bb</sub> travels over the Andes, however, it is oxidized. Therefore, CO west of the northern part of the continent is smaller in the ne30 × 4 simulation than in the control run.

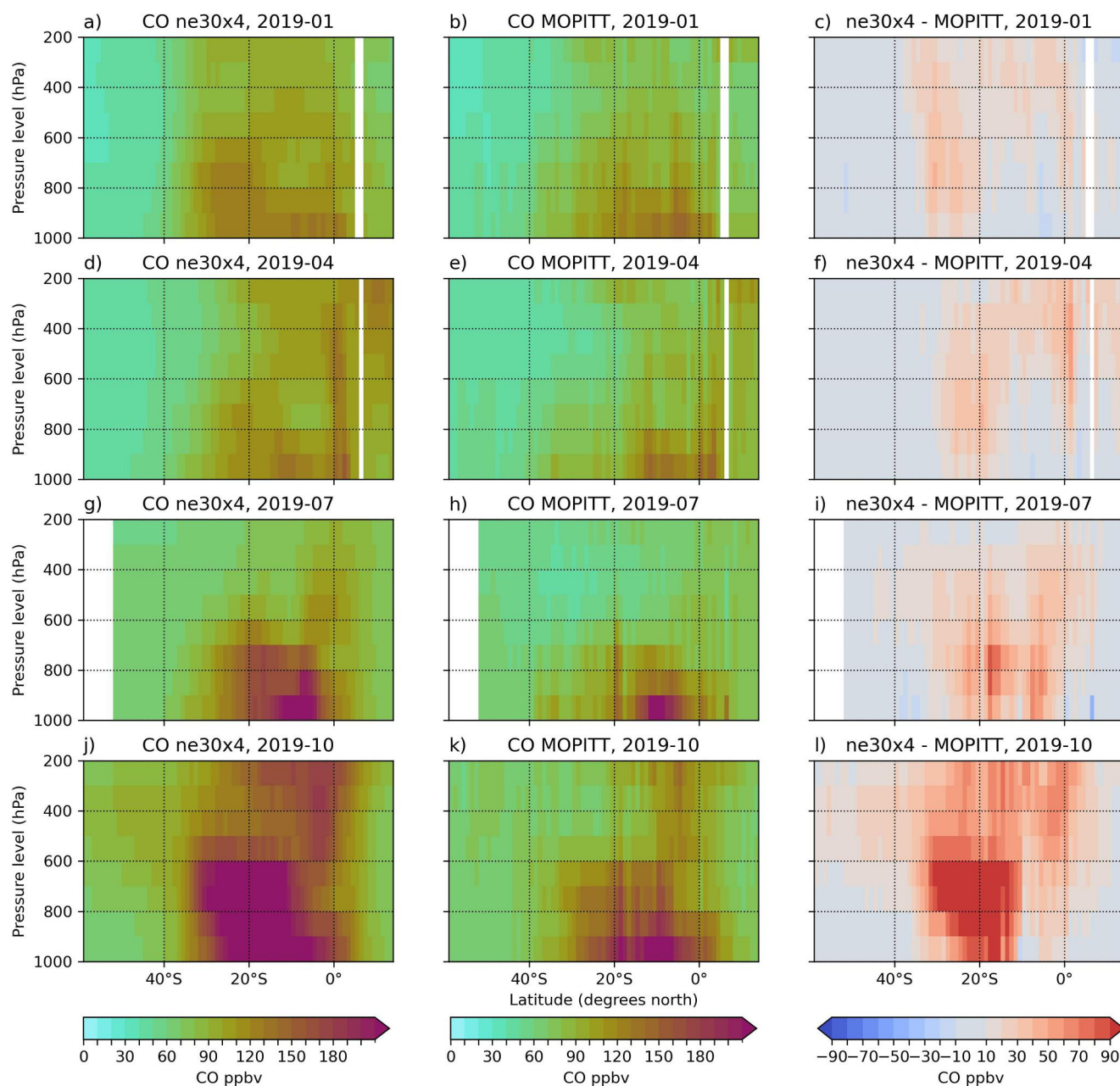


**Figure 4.** Evaluation of the vertical distribution of CO in the model compared to MOPITT for the month of January, April, July and October at a fixed longitude of 60°W. The model CO is calculated by regridding to the MOPITT L3 grid and using the MOPITT averaging kernel. The white stripes represent missing satellite data.

### 3.3. CO Tag Contribution

#### 3.3.1. Global CO Tags: Annual Analysis

In Figure 6, we show the annual average concentration of CO and of each CO tag from the ne30 × 4 simulation. Most of the CO burden in the tropospheric column can be explained by either biomass burning emissions or secondary CO production. Biomass burning CO (Figure 6b) is highest in the southern part of the Amazon Basin, and high concentrations are also shown in the westward plume transport to the Pacific Ocean.

The secondary CO (Figure 6h) has maxima to the west of the Andes, over Peru and over northern Chile. This is, however, not necessarily a region with a high chemical production in the simulations. It also has relatively high OH concentrations, and the CO lifetime is, therefore, not particularly long (Figure 7).



**Table 2**  
*CO Budget During 2019 for the Global Sources of CO in Both Simulations*

CO tag	Burden (Tg)	Net budget (Tg/year)	Surf. emis. (Tg/year)	Chem prod (Tg/year)	Dry dep (Tg/year)	Chem loss (Tg/year)
<b>ne30, Global</b>						
CO	343	−53	1,400	1,839	175	3,117
CO <sub>ant</sub>	62	−28	558	−	49	536
CO <sub>bb</sub>	75	−18	734	−	68	683
CO <sub>ocn</sub>	3	−1	22	−	0.6	22
CO <sub>bio</sub>	9	−4	86	−	5	85
CO <sub>met0.75</sub>	88	−3	−	811	21	794
CO <sub>nmvoc</sub>	104	1	−	1,028	31	996
<b>ne30 × 4, Global</b>						
CO	349	−39	1,399	1,786	177	3,047
CO <sub>ant</sub>	64	−26	558	−	50	533
CO <sub>bb</sub>	79	−11	734	−	69	676
CO <sub>ocn</sub>	3	−1	20	−	0.6	20
CO <sub>bio</sub>	9	−3	87	−	5	85
CO <sub>met0.75</sub>	88	−3	−	782	21	765
CO <sub>nmvoc</sub>	105	7	−	1,005	30	967
<b>ne30, SAM</b>						
CO	23	276	244	253	35	186
CO <sub>ant</sub>	3	24	52	−	5	23
CO <sub>bb</sub>	6	97	162	−	16	49
CO <sub>bio</sub>	1	21	30	−	2	7
CO <sub>met0.75</sub>	5	−3	−	40	4	39
CO <sub>nmvoc</sub>	8	138	−	213	8	67
<b>ne30 × 4, SAM</b>						
CO	23	279	244	242	35	172
CO <sub>ant</sub>	3	24	51	−	5	22
CO <sub>bb</sub>	7	101	162	−	16	45
CO <sub>bio</sub>	1	22	30	−	2	7
CO <sub>met0.75</sub>	5	−2	−	38	4	36
CO <sub>nmvoc</sub>	8	136	−	204	8	61

*Note.* In this table, a yield of 0.75 was assumed for Secondary CO derived from methane.

In Figure 7, the mean CO chemical lifetime is shown together with the dry-air column averaged mole fraction of isoprene and OH. A longer chemical lifetime is simulated at higher latitudes because of a low OH under small solar radiation conditions. Conversely, the lifetime is shorter than 1 month in the tropics because of higher OH. The chemical lifetime of CO is relatively high in parts of the Amazon (160–180 days, compared to 30–90 days at similar latitudes outside the rainforest). As expected, the regions of long lifetime match regions of low OH. Jacob and Wofsy (1990) had already concluded that isoprene was the main OH sink over the Amazon rainforest, and Nölscher et al. (2016) reported a marked seasonality of OH reactivity modulated by biogenic emissions of NMVOCs. In the case of the rainforest, the region with long lifetimes matches almost perfectly regions of high isoprene, which is probably destroying OH and reducing the chemical loss. Biogenic emissions and meteorology are affected by changing model resolution, and since isoprene is highly sensitive to temperature and reacts quickly with OH, this effect is assumed to account for some of the differences in chemical production and loss between the refined and control runs.

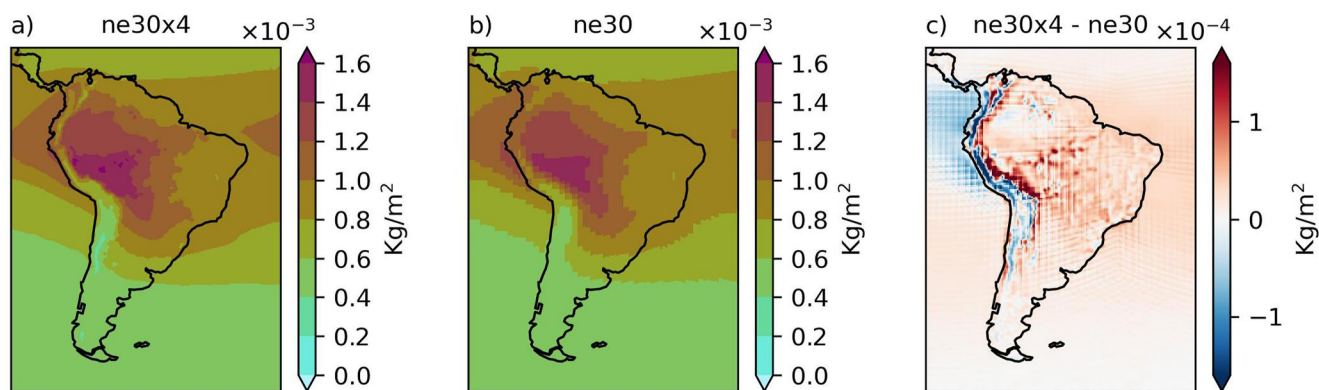


**Figure 5.** Annual mean CO burden over South America. (a)  $ne30 \times 4$  refined simulation and (b)  $ne30$  control run. The absolute difference between the two is shown in (c).

As shown in Figure 8, while CO explains a large part of the burden all year round,  $CO_{bb}$  constitutes a smaller proportion until August, and increases significantly during the biomass burning season. The  $CO_{bb}$  burden has its peak in September, and slowly decreases over the following months. While having a smaller variation,  $CO_{nmvoc}$  also has values higher than the previous months during the biomass burning season. This is likely related to the emissions of other NMVOCs during biomass burning events, although other, less obvious effects might have an influence (including the effects that the biomass burning emissions might have over OH, total radiation, etc.).

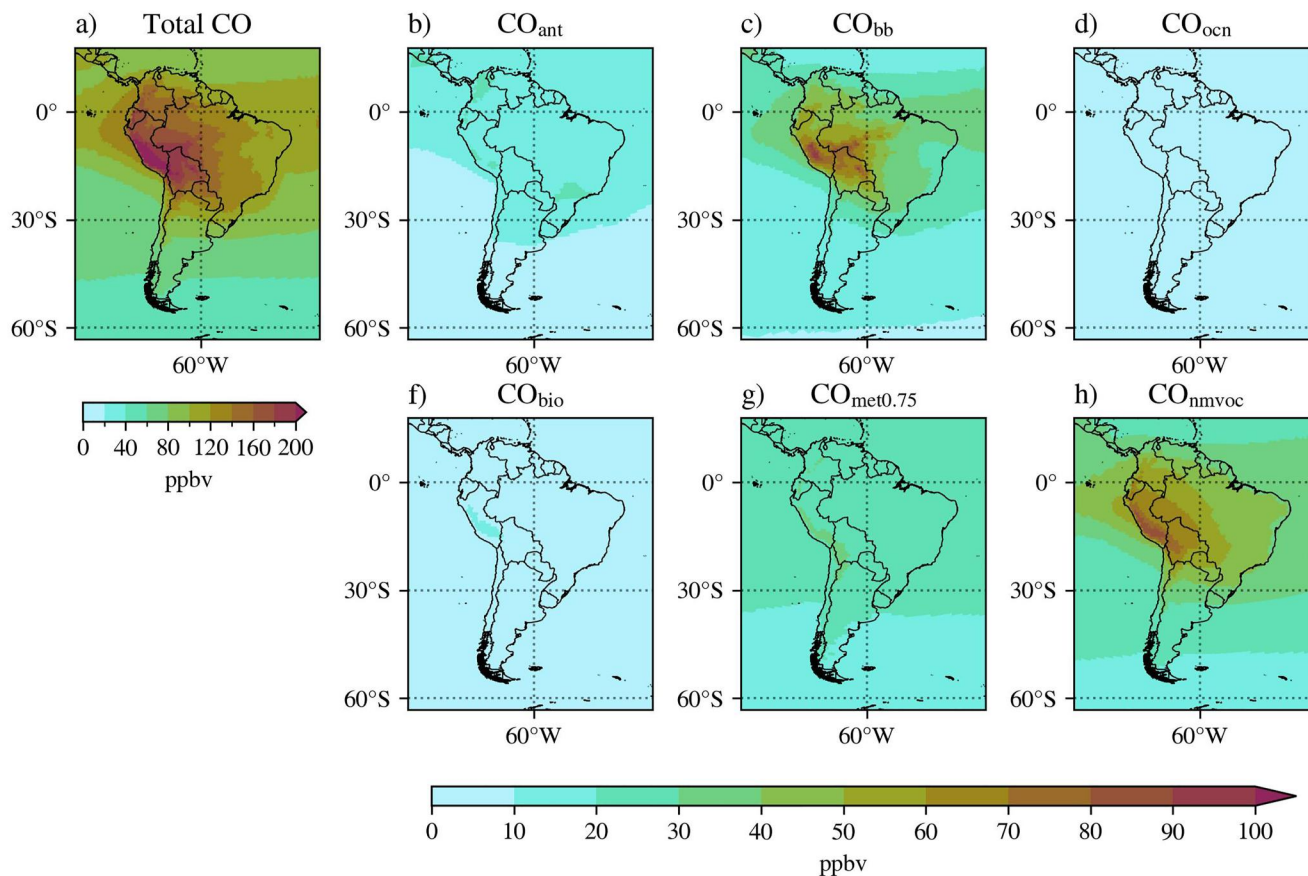


**Figure 6.** Annual mean CO tags. (a) total CO, (b) anthropogenic primary CO, (c) biomass burning primary CO, (d) ocean primary CO, (f) biogenic primary CO, (g) methane secondary CO assuming a yield of 0.75 and (h) secondary CO from other (non-methane) sources. Note the different scales between the total CO in (a) and the CO tags.

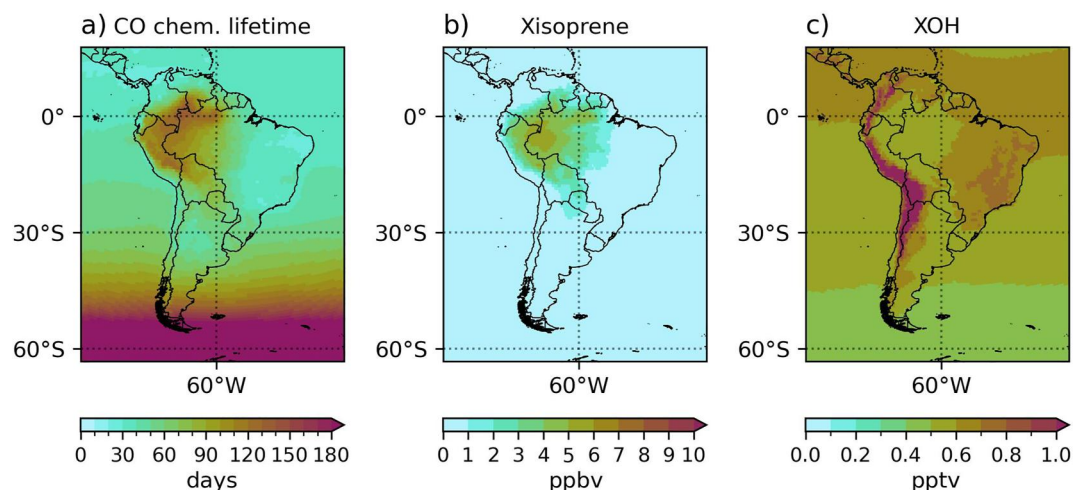


**Figure 7.** (a) Annual mean CO lifetime (2019), (b) dry-air column average mole fraction of isoprene and (c) dry-air column average mole fraction of OH.

The temporal variability of the CO monthly means (Figure 9) can be explained almost completely by biomass burning emissions.  $\text{CH}_4$  in MUSICA<sub>v0</sub> is prescribed in the lower vertical layers, which is the reason the standard deviation of  $\text{CO}_{\text{met}0.75}$  is close to 0. Notice that there might still be minor variations due to the changes in OH concentrations, however.

A noticeable fact is that there are only minor variations in  $\text{CO}_{\text{ant}}$ , and these are mostly found in the region around São Paulo. Although the variability of  $\text{CO}_{\text{bio}}$  is close to zero, the effects of most of the biogenic emissions is probably in the changes in biogenic NMVOCs, and is therefore contained within the variability of  $\text{CO}_{\text{nmvoc}}$ . Although we believe that  $\text{CO}_{\text{bb}}$  is likely overestimated in the model, its dominant role in monthly variability remains true even if the total burden of  $\text{CO}_{\text{bb}}$  would be divided by three. It is therefore reasonable to focus mostly on  $\text{CO}_{\text{bb}}$  to understand the changes and sources of CO variability over the course the year.

### 3.3.2. Temporal and Geographical Analysis of Biomass Burning Primary CO

In the right column of Figure 8 the burden of the different  $\text{CO}_{\text{bb}}$  tags are shown for selected regions. For all of SAM,  $\text{CO}_{\text{bb}}$  ranges from 16% of the total CO in January to 47% of the total CO in September. Part of the CO during the first months of the year could also be carried over from the previous year, considering that the long chemical lifetime shown in Figure 7 and that there were large fire events during 2018. However, since the total CO burden remains comparatively low, this effect was probably not very large. Looking at the individual  $\text{CO}_{\text{bb}}$  tags (see Figure 2a), it is clear that a large portion of the  $\text{CO}_{\text{bb}}$  is from Africa all year round. As a percentage of the total CO burden in all of SAM, instead of just the biomass burning burden, it ranges from 5% in November to 14% in September. This applies even to SSAM, which is furthest away from Africa. In SSAM, it is 4%–9% of the total CO burden. As a percentage of the total primary biomass burning CO burden, it is 19%–48%, and is the largest contributor up to the Amazon fires in August.

The biomass burning pattern over the Amazon (i.e., NWSAM) is clearly visible. The contribution of  $\text{CO}_{\text{bbNWSAM}}$  to the total SAM burden during September is  $\sim 10$  times larger than during May. It is worth noting that the peak of  $\text{CO}_{\text{bbNWSAM}}$  in all of SAM during September does not match the peak of  $\text{CO}_{\text{bbNWSAM}}$  in the region of NWSAM during August. This is a clear sign of the long lifetime of CO, and slower fluxes in the region, with the compound effects of CO slowly accumulating over the continent over multiple months, causing a 1-month delay in the peak. During 2019, there is also a compound effect of the SSAf and Amazonian fires, which have their maximum contribution to the burden during August and September. 2019 was a year of few biomass burning events in SSAM, which is reflected in its low contribution to the  $\text{CO}_{\text{bb}}$  burden.

Africa has two clearly distinct fire seasons, north and south of the equator. Transport from African biomass burning into the Amazon has been reported in previous studies, and its effects in the aerosol cycling have been extensively researched (Barkley et al., 2019; Holanda et al., 2023). We quantify the impact of African biomass

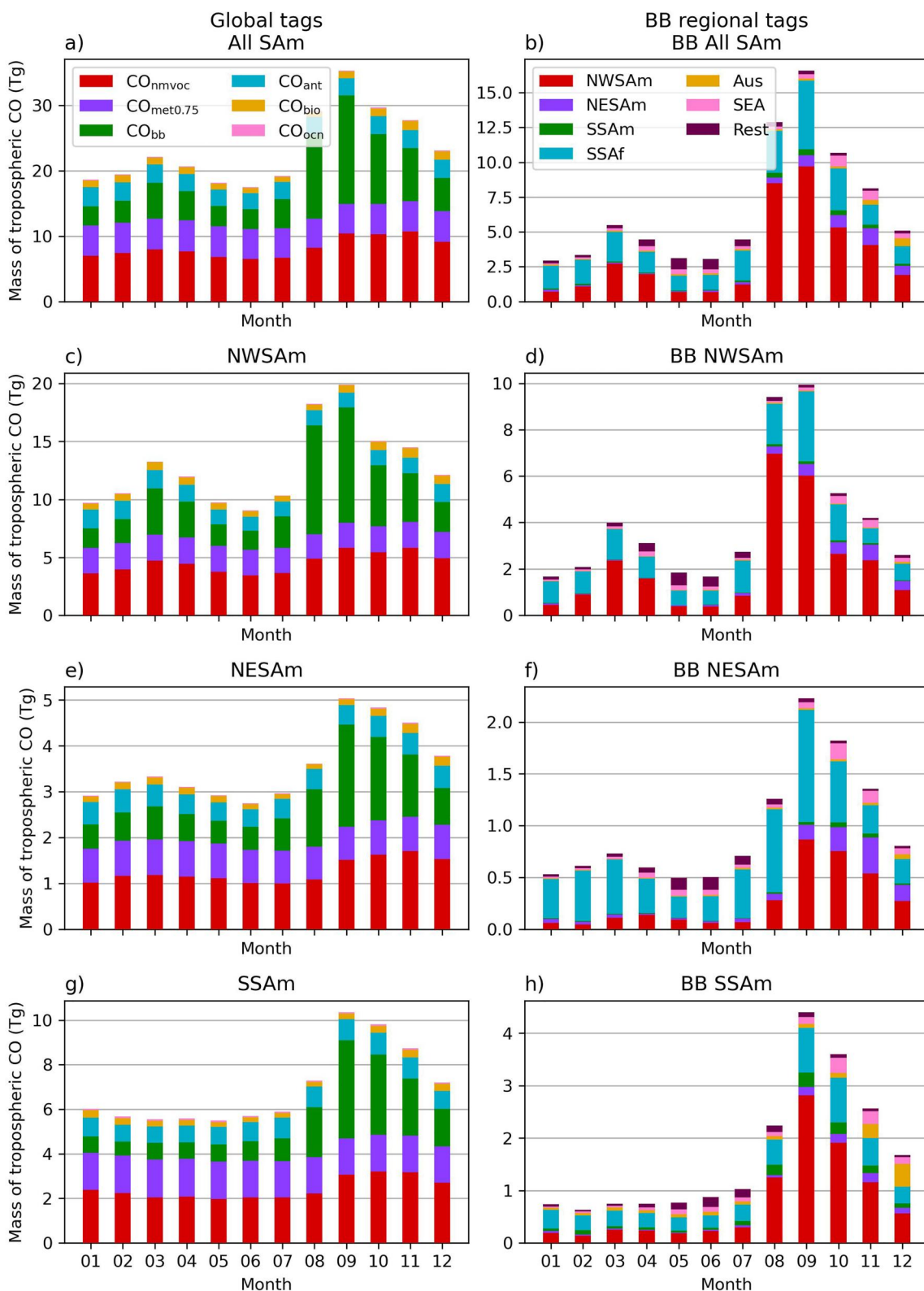


**Figure 8.** Stacked bar plot of the burden of CO for each tag. The left column represents global tags by CO source, whereas the right column represents the geographical tags for CO<sub>bb</sub>. The regions are defined as shown in Figure 2a). Note that each region has different areas and, therefore, the total burden should not be compared directly with each other. The sum of NWSAm, NESAm and SSAm does, however, equal All SAM.

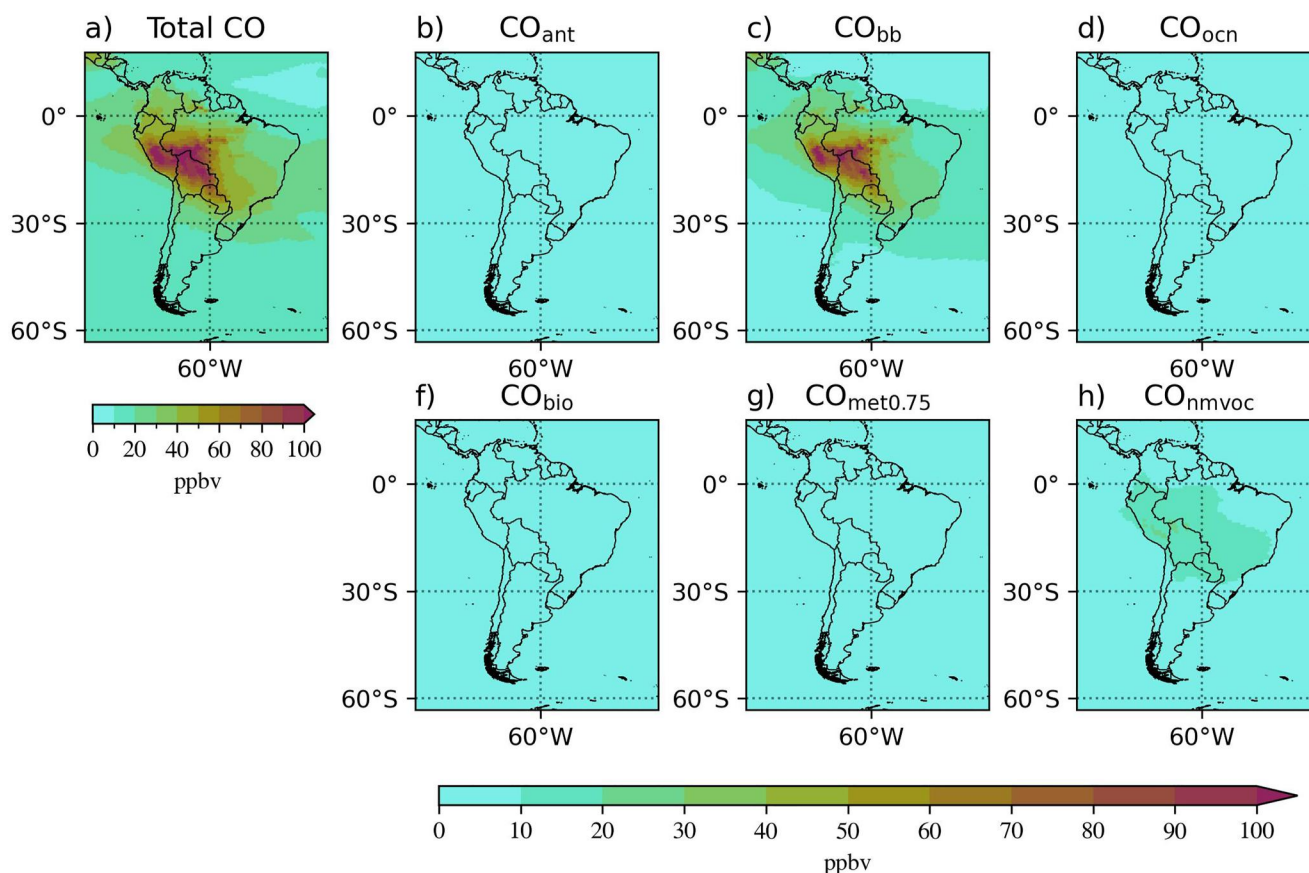


**Figure 9.** Standard deviation of the monthly means for each global CO tag. (a) is the total CO, (b) is anthropogenic primary CO, (c) is the biogenic primary CO, (d) is the ocean primary CO, (f) is the biogenic primary CO, (g) is the secondary CO derived from methane with a yield of 0.75 and (hr) is the non-methane derived secondary CO.

burning emissions for CO, and find that the African contribution to the total CO burden in NWSAm ranges from 4% in November to 15% in September. The magnitude of the effect in September is especially relevant, taking into account that it is the month with the overall largest CO burden in that region. NESAm is the entry point of fluxes from Central Africa into South America. This remains true during both African biomass burning seasons (north and south of the equator). In NESAm, the  $CO_{bbSSAf}$  burden is 79% of the total  $CO_{bb}$  in February, although this only accounts to 15% of the total CO burden in the region. In November, the month with the lowest percentage contribution, it is only about 6% of the total CO burden, but remains at 20% of the  $CO_{bb}$ .

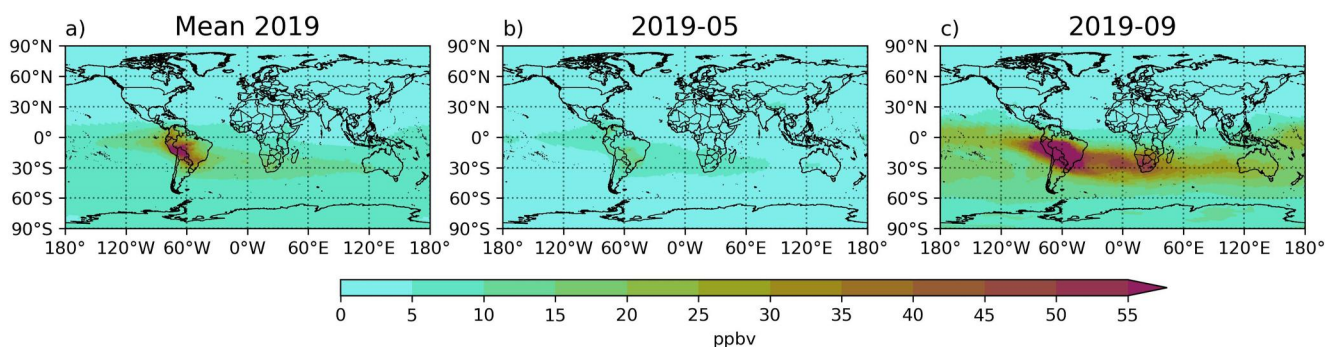


**Figure 10.** Summary of the effect of South American primary emissions over the rest of the world. In subplot (a), the yearly mean is shown. In subplot (b), we show the monthly mean for May, a month with low BB emissions, and in subplot (c), September is chosen as an example of a month with large biomass burning over the Amazon.

In SSAm, while biomass burning from NWSAm and SSAf are estimated to be predominant during most of the year, the effects of the Australian fires becomes apparent during the peak biomass burning in December 2019.

### 3.3.3. South America's Effect on the Rest of the World

In Figure 10 we demonstrate the effects of the South American CO primary emissions on the rest of the world. During the biomass burning season, SAM primary emissions can increase the CO concentration considerably in the entire Southern Hemisphere, with a large effect over the southern tip of Africa (up to 50 ppbv in the column averaged mole fraction in our simulation, which accounts for about 30% of the total CO concentration). Following wind patterns, CO travels toward the Pacific Ocean in the northeast, and toward the west over the Atlantic at about 15°S–30°S of the continent. The results also show effects over SEA and Australia, reaching up to 30 ppbv during October (~25% of the total CO concentration over these regions).

The effects over the Northern Hemisphere are overall minor and are limited to the oceans or close to the equator because of the much higher CO contributions from NH sources. Figure 10 shows a relatively strong flux of CO from the northern Amazon into the tropical Pacific Ocean.

The CO that is transported to the tropical Pacific gets well mixed zonally, and some of it might reenter the continent from the east.

## 4. Conclusions

The main conclusions from this paper can be summarized as follows.

1. We present the first application and evaluation of MUSICAv0 to the entire South American continent. Our refined grid (ne30 × 4) includes a global 1° × 1° model with a refinement up to 28 km over South America. We present the results for the year 2019 and evaluate the impact of the refined grid. The simulated trace gases and dynamics are comparable to the standard configuration of CAM-Chem with a spectral element dynamical core and standard grid configuration (ne30).
2. We quantify the CO budget for the year 2019, and characterize the contribution from different emission/chemical sources and geographical origin using CO tags. The biomass burning emissions play an overwhelming role in the continental budget, and are the main factor of monthly variability. They also explain the majority of the temporal variability in CO columns. However, our comparison with MOPITT suggests that FINN2.5 is overestimating biomass burning emissions in the Southern Hemisphere. The main points of this study remain robust even if the estimated biomass burning CO budget is divided by three.
3. The effects of the model spatial resolution leads to minor changes in the CO budget, driven by changes in the chemical production and loss. Higher resolution implies more localized biogenic emissions of multiple species (including isoprene), which in turn affects OH. There are also minor variations in the temperature, which can have a large effect on isoprene emissions. Changes in temperature and other meteorological parameters will also affect atmospheric chemistry, for instance, by its effects on reaction and deposition rates.
4. Biomass burning activities in Africa are a relevant source of CO in all of SAM, including the South. This is the case during for all seasons, in the early months of 2019 we find a cross-equatorial flux of African biomass sources. Outside of the Amazon biomass burning season, they represent the largest source of CO<sub>bb</sub>.
5. CO is estimated to have a long chemical lifetime over the Amazon in our simulations, determined by low OH concentrations. This is likely due to large isoprene emissions. The biogenic emissions over the Amazon are a significant source of CO. As VOC emitters, they are a relevant source of secondary CO. At the same time, they destroy OH, leading to a longer chemical lifetime, but lower chemical production and loss. Further study is needed to understand the exact net effect, and would require a more complex tagged CO production from biogenic NMVOCs to be included in the model.
6. SAM's primary emissions are relevant contributors to CO in the SH, but show only minor influence on the NH. The largest effects in the SH are over the southern tip of Africa, with smaller but relevant effects over the Maritime Continent, New Zealand, Australia and South East Asia.

### 4.1. Future Perspectives

Understanding the CO budget and chemistry in South America is far from a well characterized problem yet is essential to understanding air quality and human and environmental impacts. Due to the high variability of the

sources, similar studies as this one but extended to larger time periods are needed to gain a more complete comprehension of South America's CO budget.

For modeling studies, there is a need to further tackle the emission inventories, understand sources of model biases and correct for them. Some useful and important work has been done in regard to improving anthropogenic inventories (Castesana et al., 2022; Ibarra-Espinosa et al., 2018; Álamos et al., 2022), but there is no regionally concerted effort to maintain a high quality anthropogenic emission inventory for the whole region which is regularly updated. As shown in this paper, at the same time tackling uncertainties in biomass burning sources is of very high importance.

Measurement campaigns have been performed in different parts of the continent, but there are few operational urban air quality stations and even fewer over remote sites. These sites are located mostly in the Amazon, parts of Chile, and Colombia. There are also relevant observatories, like the Amazon Tall Tower Observatory, the Chacaltaya and the Ushuaia GAW stations. However, coverage is rather sparse and there are many regions without relevant observations. In addition, data access and availability is a major obstacle, for example, Argentina lacks a centralized database to access available data.

With the formation of the Latin America Early Career Earth System Scientist Network (Yáñez-Serrano et al., 2022) and the Southern Hemisphere Working Group of the International Global Atmospheric Chemistry (IGAC) project (Paton-Walsh et al., 2022), a stronger scientific community is starting to focus on the region.

Further studies and observations are needed, especially in the southern part of the continent (i.e., SSAm). There, there is also a large amount of small fires that might not be captured by the satellites, and large territories with no observation sites, which could provide useful information on CO chemistry and air quality in general.

## Data Availability Statement

CESM2.2 (including MUSICAv0) is a publicly released version of the Community Earth System Model that is available at <https://www.cesm.ucar.edu/> (last access: 15 March 2023). The MERRA-2 data (Tilmes, 2022) and FINN2.5 (Wiedinmyer & Emmons, 2022) are available at the National Center for Atmospheric Research's Research Data Archive. The CAMS-GLOB-ANT v5.3 and CAMS-GLOB-AIR v2.1 anthropogenic emissions are available at Soulie et al. (2022). The MOPITT gridded monthly means are available at NASA/LARC/SD/ASDC (2023). NOAA's Carbon Cycle Greenhouse Gas data are available at Petron et al. (2019).

## References

- Álamos, N., Huneus, N., Opazo, M., Osses, M., Puja, S., Pantoja, N., et al. (2022). High-resolution inventory of atmospheric emissions from transport, industrial, energy, mining and residential activities in Chile. *Earth System Science Data*, 14(1), 361–379. <https://doi.org/10.5194/essd-14-361-2022>
- Barkley, A. E., Prospero, J. M., Mahowald, N., Hamilton, D. S., Pependorf, K. J., Oehlert, A. M., et al. (2019). African biomass burning is a substantial source of phosphorus deposition to the Amazon, Tropical Atlantic Ocean, and Southern Ocean. *Proceedings of the National Academy of Sciences*, 116(33), 16216–16221. <https://doi.org/10.1073/pnas.1906091116>
- Bogenschutz, P. A., Gettelman, A., Morrison, H., Larson, V. E., Craig, C., & Schanen, D. P. (2013). Higher-order turbulence closure and its impact on climate simulations in the community atmosphere model. *Journal of Climate*, 26(23), 9655–9676. <https://doi.org/10.1175/jcli-d-13-00075.1>
- Buchholz, R. R., Worden, H. M., Park, M., Francis, G., Deeter, M. N., Edwards, D. P., et al. (2021). Air pollution trends measured from terra: CO and AOD over industrial, fire-prone, and background regions. *Remote Sensing of Environment*, 256, 112275. <https://doi.org/10.1016/j.rse.2020.112275>
- Castesana, P., Resquin, M. D., Huneus, N., Puliafito, E., Darras, S., Gómez, D., et al. (2022). PAPILA dataset: A regional emission inventory of reactive gases for SouthSouth America based on the combination of local and global information. *Earth System Science Data*, 14(1), 271–293. <https://doi.org/10.5194/essd-14-271-2022>
- Danabasoglu, G., Lamarque, J.-F., Bacmeister, J., Bailey, D. A., DuVivier, A. K., Edwards, J., et al. (2020). The community earth system model version 2 (CESM2). *Journal of Advances in Modeling Earth Systems*, 12(2). <https://doi.org/10.1029/2019ms001916>
- Daskalakis, N., Gallardo, L., Kanakidou, M., Nüß, J. R., Menares, C., Rondanelli, R., et al. (2022). Impact of biomass burning and stratospheric intrusions in the remote South Pacific Ocean troposphere. *Atmospheric Chemistry and Physics*, 22(6), 4075–4099. <https://doi.org/10.5194/acp-22-4075-2022>
- Dekker, I. N., Houweling, S., Aben, I., Röckmann, T., Krol, M., Martínez-Alonso, S., et al. (2017). Quantification of CO emissions from the city of Madrid using MOPITT satellite retrievals and WRF simulations. *Atmospheric Chemistry and Physics*, 17(23), 14675–14694. <https://doi.org/10.5194/acp-17-14675-2017>
- de Miranda, P. L. S., Dexter, K. G., Swaine, M. D., de Oliveira-Filho, A. T., Hardy, O. J., & Fayolle, A. (2022). Dissecting the difference in tree species richness between Africa and South America. *Proceedings of the National Academy of Sciences*, 119(14). <https://doi.org/10.1073/pnas.2112336119>
- Duncan, B. N., Logan, J. A., Bey, I., Megretskaia, I. A., Yantosca, R. M., Novelli, P. C., et al. (2007). Global budget of CO, 1988–1997: Source estimates and validation with a global model. *Journal of Geophysical Research*, 112(D22). <https://doi.org/10.1029/2007jd008459>

## Acknowledgments

This material is based upon work supported by the National Center for Atmospheric Research, which is a major facility sponsored by the National Science Foundation under Cooperative Agreement No. 1852977. Computing resources were provided by NSF NCAR's Computational and Information Systems Laboratory (CISL). This work also used resources of the Deutsches Klimarechenzentrum (DKRZ) granted by its Scientific Steering Committee (WLA) under project IDs bm1234 and mh0735. The authors would also like to acknowledge the EU Horizon 2020 Marie Skłodowska-Curie project PAPILA (Grant 777544; MSCA action for research and innovation staff exchange). Open Access funding enabled and organized by Projekt DEAL.

- Edwards, D. P., Emmons, L. K., Hauglustaine, D. A., Chu, D. A., Gille, J. C., Kaufman, Y. J., et al. (2004). Observations of carbon monoxide and aerosols from the terra satellite: Northern hemisphere variability. *Journal of Geophysical Research*, *109*(D24). <https://doi.org/10.1029/2004jd004727>
- Emmons, L. K., Schwantes, R. H., Orlando, J. J., Tyndall, G., Kinnison, D., Lamarque, J.-F., et al. (2020). The chemistry mechanism in the community earth system model version 2 (CESM2). *Journal of Advances in Modeling Earth Systems*, *12*(4). <https://doi.org/10.1029/2019ms001882>
- Fisher, J. A., Murray, L. T., Jones, D. B. A., & Deutscher, N. M. (2017). Improved method for linear carbon monoxide simulation and source attribution in atmospheric chemistry models illustrated using GEOS-Chem v9. *Geoscientific Model Development*, *10*(11), 4129–4144. <https://doi.org/10.5194/gmd-10-4129-2017>
- Fisher, R. A., & Koven, C. D. (2020). Perspectives on the future of land surface models and the challenges of representing complex terrestrial systems. *Journal of Advances in Modeling Earth Systems*, *12*(4). <https://doi.org/10.1029/2018ms001453>
- Gaubert, B., Arellano, A. F., Barré, J., Worden, H. M., Emmons, L. K., Tilmes, S., et al. (2016). Toward a chemical reanalysis in a coupled chemistry-climate model: An evaluation of MOPITT CO assimilation and its impact on tropospheric composition. *Journal of Geophysical Research: Atmospheres*, *121*(12), 7310–7343. <https://doi.org/10.1002/2016jd024863>
- Gaubert, B., Edwards, D. P., Anderson, J. L., Arellano, A. F., Barré, J., Buchholz, R. R., et al. (2023). Global scale inversions from MOPITT CO and MODIS AOD. *Remote Sensing*, *15*(19), 4813. <https://doi.org/10.3390/rs15194813>
- Gaubert, B., Emmons, L. K., Raeder, K., Tilmes, S., Miyazaki, K., Jr., & Arellano, Jr., A. F. (2020). Correcting model biases of CO in East Asia: Impact on oxidant distributions during KORUS-AQ. *Atmospheric Chemistry and Physics*, *20*(23), 14617–14647. <https://doi.org/10.5194/acp-20-14617-2020>
- Gaubert, B., Worden, H. M., Arellano, A. F. J., Emmons, L. K., Tilmes, S., Barré, J., et al. (2017). Chemical feedback from decreasing carbon monoxide emissions. *Geophysical Research Letters*, *44*(19), 9985–9995. <https://doi.org/10.1002/2017gl074987>
- Gelaro, R., McCarty, W., Suárez, M. J., Todling, R., Molod, A., Takacs, L., et al. (2017). The Modern-Era Retrospective analysis for research and applications, version 2 (MERRA-2). *Journal of Climate*, *30*(14), 5419–5454. <https://doi.org/10.1175/jcli-d-16-0758.1>
- Gettelman, A., & Morrison, H. (2015). Advanced two-moment bulk microphysics for global models. Part i: Off-line tests and comparison with other schemes. *Journal of Climate*, *28*(3), 1268–1287. <https://doi.org/10.1175/jcli-d-14-00102.1>
- Grant, A., Archibald, A. T., Cooke, M. C., & Shallcross, D. E. (2010). Modelling the oxidation of seventeen volatile organic compounds to track yields of CO and CO<sub>2</sub>. *Atmospheric Environment*, *44*(31), 3797–3804. <https://doi.org/10.1016/j.atmosenv.2010.06.049>
- Guenther, A. B., Jiang, X., Heald, C. L., Sakulyanontvittaya, T., Duhl, T., Emmons, L. K., & Wang, X. (2012). The model of emissions of gases and aerosols from nature version 2.1 (MEGAN2.1): An extended and updated framework for modeling biogenic emissions. *Geoscientific Model Development*, *5*(6), 1471–1492. <https://doi.org/10.5194/gmd-5-1471-2012>
- Hedelius, J. K., Toon, G. C., Buchholz, R. R., Iraci, L. T., Podolske, J. R., Roehl, C. M., et al. (2021). Regional and urban column CO trends and anomalies as observed by MOPITT over 16 years. *Journal of Geophysical Research: Atmospheres*, *126*(5). <https://doi.org/10.1029/2020jd033967>
- Holanda, B. A., Franco, M. A., Walter, D., Artaxo, P., Carbone, S., Cheng, Y., et al. (2023). African biomass burning affects aerosol cycling over the amazon. *Communications Earth & Environment*, *4*(1), 154. <https://doi.org/10.1038/s43247-023-00795-5>
- Ibarra-Espinosa, S., Ynoue, R., O'Sullivan, S., Pebesma, E., de Fátima Andrade, M., & Osses, M. (2018). VEIN v0.2.2: An R package for bottom-up vehicular emissions inventories. *Geoscientific Model Development*, *11*(6), 2209–2229. <https://doi.org/10.5194/gmd-11-2209-2018>
- Jacob, D. J., & Wofsy, S. C. (1990). Budgets of reactive nitrogen, hydrocarbons, and ozone over the amazon forest during the wet season. *Journal of Geophysical Research*, *95*(D10), 16737–16754. <https://doi.org/10.1029/jd095id10p16737>
- Jo, D. S., Emmons, L. K., Callaghan, P., Tilmes, S., Woo, J.-H., Kim, Y., et al. (2023). Comparison of urban air quality simulations during the KORUS-AQ campaign with regionally refined versus global uniform grids in the multi-scale infrastructure for chemistry and aerosols (MUSICA) version 0. *Journal of Advances in Modeling Earth Systems*, *15*(7). <https://doi.org/10.1029/2022ms003458>
- Jo, D. S., Hodzic, A., Emmons, L. K., Tilmes, S., Schwantes, R. H., Mills, M. J., et al. (2021). Future changes in isoprene-epoxydiol-derived secondary organic aerosol (IEPOX SOA) under the shared socioeconomic pathways: The importance of physicochemical dependency. *Atmospheric Chemistry and Physics*, *21*(5), 3395–3425. <https://doi.org/10.5194/acp-21-3395-2021>
- Lamarque, J.-F., Emmons, L. K., Hess, P. G., Heald, C. L., Holland, E. A., Lauritzen, P. H., et al. (2012). CAM-Chem: Description and evaluation of interactive atmospheric chemistry in the community earth system model. *Geoscientific Model Development*, *5*(2), 369–411. <https://doi.org/10.5194/gmd-5-369-2012>
- Lauritzen, P. H., Nair, R. D., Herrington, A. R., Callaghan, P., Goldhaber, S., Dennis, J. M., et al. (2018). NCAR release of CAM-SE in CESM2.0: A reformulation of the spectral element dynamical core in dry-mass vertical coordinates with comprehensive treatment of condensates and energy. *Journal of Advances in Modeling Earth Systems*, *10*(7), 1537–1570. <https://doi.org/10.1029/2017ms001257>
- Lawrence, D. M., Fisher, R. A., Koven, C. D., Oleson, K. W., Swenson, S. C., Bonan, G., et al. (2019). The community land model version 5: Description of new features, benchmarking, and impact of forcing uncertainty. *Journal of Advances in Modeling Earth Systems*, *11*(12), 4245–4287. <https://doi.org/10.1029/2018ms001583>
- Levy, H. (1971). Normal atmosphere: Large radical and formaldehyde concentrations predicted. *Science*, *173*(3992), 141–143. <https://doi.org/10.1126/science.173.3992.141>
- Liu, X., Ma, P.-L., Wang, H., Tilmes, S., Singh, B., Easter, R. C., et al. (2016). Description and evaluation of a new four-mode version of the modal aerosol module (MAM4) within version 5.3 of the community atmosphere model. *Geoscientific Model Development*, *9*(2), 505–522. <https://doi.org/10.5194/gmd-9-505-2016>
- Müller, J.-F., Stavrou, T., Bauwens, M., George, M., Hurtmans, D., Coheur, P.-F., et al. (2018). Top-down CO emissions based on IASI observations and hemispheric constraints on OH levels. *Geophysical Research Letters*, *45*(3), 1621–1629. <https://doi.org/10.1002/2017gl076697>
- Naik, V., Voulgarakis, A., Fiore, A. M., Horowitz, L. W., Lamarque, J.-F., Lin, M., et al. (2013). Preindustrial to present-day changes in tropospheric hydroxyl radical and methane lifetime from the Atmospheric Chemistry and Climate Model Intercomparison (ACCMIP). *Atmospheric Chemistry and Physics*, *13*(10), 5277–5298. <https://doi.org/10.5194/acp-13-5277-2013>
- NASA/LARC/SD/ASDC. (2023). Mopitt co gridded monthly means (near and thermal infrared radiances) v009 [Dataset]. *NASA Langley Atmospheric Science Data Center DAAC*. <https://doi.org/10.5067/TERRA/MOPITT/MOP03JM.009>
- Naus, S., Domingues, L. G., Krol, M., Luijckx, I. T., Gatti, L. V., Miller, J. B., et al. (2022). Sixteen years of MOPITT satellite data strongly constrain Amazon CO fire emissions. *Atmospheric Chemistry and Physics*, *22*(22), 14735–14750. <https://doi.org/10.5194/acp-22-14735-2022>
- Nölscher, A. C., Yañez-Serrano, A. M., Wolff, S., de Araujo, A. C., Lavrič, J. V., Kesselmeier, J., & Williams, J. (2016). Unexpected seasonality in quantity and composition of amazon rainforest air reactivity. *Nature Communications*, *7*(1), 10383. <https://doi.org/10.1038/ncomms10383>



- Novelli, P. C., Masarie, K. A., Lang, P. M., Hall, B. D., Myers, R. C., & Elkins, J. W. (2003). Reanalysis of tropospheric CO trends: Effects of the 1997–1998 wildfires. *Journal of Geophysical Research*, *108*(D15). <https://doi.org/10.1029/2002jd003031>
- Park, K., Emmons, L. K., Wang, Z., & Mak, J. E. (2013). Large interannual variations in nonmethane volatile organic compound emissions based on measurements of carbon monoxide. *Geophysical Research Letters*, *40*(1), 221–226. <https://doi.org/10.1029/2012gl052303>
- Paton-Walsh, C., Emmerson, K. M., Garland, R. M., Keywood, M., Hoelzemann, J. J., Huneus, N., et al. (2022). Key challenges for tropospheric chemistry in the Southern Hemisphere. *Elementa: Science of the Anthropocene*, *10*(1). <https://doi.org/10.1525/elementa.2021.00050>
- Petron, G., Crotwell, A., Crotwell, M. J., Dlugokencky, E., Madronich, M., Moglia, E., et al. (2019). Earth system research laboratory carbon cycle and Greenhouse gases Group flask-air sample measurements of CO at global and regional background sites, 1967–present [Dataset]. *NOAA ESRL GML CCGG Group*. <https://doi.org/10.15138/33BV-S284>
- Pfister, G. G., Eastham, S. D., Arellano, A. F., Aumont, B., Barsanti, K. C., Barth, M. C., et al. (2020). The multi-scale infrastructure for chemistry and aerosols (MUSICA). *Bulletin of the American Meteorological Society*, *101*(10), E1743–E1760. <https://doi.org/10.1175/bams-d-19-0331.1>
- Pfister, G. G., Emmons, L. K., Hess, P. G., Lamarque, J.-F., Orlando, J. J., Walters, S., et al. (2008). Contribution of isoprene to chemical budgets: A model tracer study with the NCAR ctm MOZART-4. *Journal of Geophysical Research*, *113*(D5). <https://doi.org/10.1029/2007jd008948>
- Schwantes, R. H., Lacey, F. G., Tilmes, S., Emmons, L. K., Lauritzen, P. H., Walters, S., et al. (2022). Evaluating the impact of chemical complexity and horizontal resolution on tropospheric ozone over the conterminous US with a global variable resolution chemistry model. *Journal of Advances in Modeling Earth Systems*, *14*(6). <https://doi.org/10.1029/2021ms002889>
- Seinfeld, J. H., & Pandis, S. N. (2016). *Atmospheric chemistry and physics: From air pollution to climate change*. John Wiley and Sons.
- Shindell, D. T., Faluvegi, G., Stevenson, D. S., Emmons, L. K., Krol, M. C., Emmons, L. K., Lamarque, J.-F., et al. (2006). Multimodel simulations of carbon monoxide: Comparison with observations and projected near-future changes. *Journal of Geophysical Research*, *111*(D19). <https://doi.org/10.1029/2006jd007100>
- Soulie, A., Granier, C., Darras, S., Zilbermann, N., Doumbia, T., Guevara, M., et al. (2023). Global anthropogenic emissions (CAM5-GLOB-ANT) for the copernicus atmosphere monitoring service simulations of air quality forecasts and reanalyses. *Earth System Science Data Discussions*. <https://doi.org/10.5194/essd-2023-306>
- Soulie, A., Granier, C., Darras, S., Zilbermann, N., Doumbia, T., Guevara, M., et al. (2022). Global anthropogenic emissions (CAM5-GLOB-ANT) for the copernicus atmosphere monitoring service simulations of air quality forecasts and reanalyses [Dataset]. *Emissions of Atmospheric Compounds and Compilation of Ancillary Data*. <https://doi.org/10.24380/eets-qd81>
- Stein, O., Schultz, M. G., Bouarar, I., Clark, H., Huijnen, V., Gaudel, A., et al. (2014). On the wintertime low bias of Northern Hemisphere carbon monoxide found in global model simulations. *Atmospheric Chemistry and Physics*, *14*(17), 9295–9316. <https://doi.org/10.5194/acp-14-9295-2014>
- Stone, D., Whalley, L. K., & Heard, D. E. (2012). Tropospheric OH and HO<sub>2</sub> radicals: Field measurements and model comparisons. *Chemical Society Reviews*, *41*(19), 6348. <https://doi.org/10.1039/c2cs35140d>
- Tang, W., Emmons, L. K., Buchholz, R. R., Wiedinmyer, C., Schwantes, R. H., He, C., et al. (2022). Effects of fire diurnal variation and plume rise on U.S. air quality during FIREX-AQ and WE-CAN based on the Multi-Scale Infrastructure for Chemistry and Aerosols (MUSICAv0). *Journal of Geophysical Research: Atmospheres*, *127*(16). <https://doi.org/10.1029/2022jd036650>
- Tang, W., Emmons, L. K., Jr, A. F. A., Gaubert, B., Knot, C., Tilmes, S., et al. (2019). Source contributions to carbon monoxide concentrations during KORUS-AQ based on CAM-chem model applications. *Journal of Geophysical Research: Atmospheres*, *124*(5), 2796–2822. <https://doi.org/10.1029/2018jd029151>
- Tang, W., Emmons, L. K., Worden, H. M., Kumar, R., He, C., Gaubert, B., et al. (2023). Application of the multi-scale infrastructure for chemistry and aerosols version 0 (MUSICAv0) for air quality research in africa. *Geoscientific Model Development*, *16*(20), 6001–6028. <https://doi.org/10.5194/gmd-16-6001-2023>
- Tilmes, S. (2022). MERRA2 global forcing data for CESM2 applications [Dataset]. *Boulder CO: Research Data Archive at the National Center for Atmospheric Research, Computational and Information Systems Laboratory*. <https://doi.org/10.5065/H9NM-XC59>
- Tilmes, S., Hodzic, A., Emmons, L. K., Mills, M. J., Gettelman, A., Kinnison, D. E., et al. (2019). Climate forcing and trends of organic aerosols in the community earth system model (CESM2). *Journal of Advances in Modeling Earth Systems*, *11*(12), 4323–4351. <https://doi.org/10.1029/2019ms001827>
- van der Werf, G. R., Randerson, J. T., Giglio, L., Collatz, G. J., Mu, M., Kasibhatla, P. S., et al. (2010). Global fire emissions and the contribution of deforestation, savanna, forest, agricultural, and peat fires (1997–2009). *Atmospheric Chemistry and Physics*, *10*(23), 11707–11735. <https://doi.org/10.5194/acp-10-11707-2010>
- Watson, C. E., Fishman, J., & Reichle, H. G. (1990). The significance of biomass burning as a source of carbon monoxide and ozone in the southern hemisphere tropics: A satellite analysis. *Journal of Geophysical Research*, *95*(D10), 16443–16450. <https://doi.org/10.1029/jd095id10p16443>
- Wiedinmyer, C., Akagi, S. K., Yokelson, R. J., Emmons, L. K., Al-Saadi, J. A., Orlando, J. J., & Soja, A. J. (2011). The fire INventory from NCAR (FINN): A high resolution global model to estimate the emissions from open burning. *Geoscientific Model Development*, *4*(3), 625–641. <https://doi.org/10.5194/gmd-4-625-2011>
- Wiedinmyer, C., & Emmons, L. (2022). Fire inventory from NCAR version 2 fire emission [Dataset]. *Boulder CO: Research Data Archive at the National Center for Atmospheric Research, Computational and Information Systems Laboratory*. <https://doi.org/10.5065/XNPA-AF09>
- Wiedinmyer, C., Kimura, Y., McDonald-Buller, E. C., Emmons, L. K., Buchholz, R. R., Tang, W., et al. (2023). The fire inventory from NCAR version 2.5: An updated global fire emissions model for climate and chemistry applications. *Geoscientific Model Development*, *16*(13), 3873–3891. <https://doi.org/10.5194/gmd-16-3873-2023>
- Yáñez-Serrano, A. M., Aguilos, M., Barbosa, C., Bolaño-Ortiz, T. R., Carbone, S., Díaz-López, S., et al. (2022). The Latin america early career earth system scientist network (LAECESS): Addressing present and future challenges of the upcoming generations of scientists in the region. *npj Climate and Atmospheric Science*, *5*(1), 79. <https://doi.org/10.1038/s41612-022-00300-3>
- Zhang, G., & McFarlane, N. A. (1995). Sensitivity of climate simulations to the parameterization of cumulus convection in the Canadian climate centre general circulation model. *Atmosphere-Ocean*, *33*(3), 407–446. <https://doi.org/10.1080/07055900.1995.9649539>
- Zheng, B., Ciais, P., Chevallier, F., Chuvieco, E., Chen, Y., & Yang, H. (2021). Increasing forest fire emissions despite the decline in global burned area. *Science Advances*, *7*(39). <https://doi.org/10.1126/sciadv.abh2646>